Structured Weyl Points in Spin-Orbit Coupled Fermionic Superfluids

Yong Xu, Fan Zhang, and Chuanwei Zhang[*]
Department of Physics, University of Texas at Dallas, Richardson, Texas 75080, USA

We demonstrate that a Weyl point, widely examined in 3D Weyl semimetals and superfluids, can develop a pair of nondegenerate gapless spheres. Such a *bouquet of two spheres* is characterized by *three distinct* topological invariants of manifolds with full energy gaps, i.e., the Chern number of a 0D point inside one developed sphere, the winding number of a 1D loop around the original Weyl point, and the Chern number of a 2D surface enclosing the whole bouquet. We show that such structured Weyl points can be realized in the superfluid quasiparticle spectrum of a 3D degenerate Fermi gas subject to spin-orbit couplings and Zeeman fields, which supports Fulde-Ferrell superfluids as the ground state.

Weyl fermions [1] were initially conceived to describe neutrinos in particle physics. Although neutrinos may have mass, the standard model of particle physics permits the existence of such chiral fermions in quarks and leptons [2]. Recently, Weyl fermions have been widely examined in a class of solid-state materials dubbed Weyl semimetals [3–15]. Remarkably, these semimetals can be described by a Weyl Hamiltonian near their unusual Weyl points, where two linearly dispersed bands cross. Impressively, such Weyl points have been experimentally observed in a photonic crystal [16] and a Weyl semimetal TaAs [17,18]. A Weyl point can also be regarded as a monopole in 3D momentum space that exhibits an integer topological charge, i.e., the quantized first Chern number of a surface enclosing the singularity. Weyl points were also suggested to exist in the quasiparticle spectrum of superfluid ^{3}He A phase [2]. In contrast to traditional fully gapped superfluids, the Weyl superfluids bear doubly degenerate nodes pinned to zero energy, around which the quasiparticle energies disperse linearly in all directions. Most recently, the existence of such Weyl nodes has also been generalized to various cold-atom superfluids and solid-state superconductors [19–28].

In this Letter, we investigate whether a Weyl point can develop a nontrivial structure at zero energy and whether a topological property protecting the developed structure exists. (i) We first consider a toy model to examine the possibility for a Weyl point to develop a gapless structure. Mathematically, the structured Weyl point can be viewed as a bouquet of two spheres (or wedge of two spheres) [29], which is a new class of topological state that has not been explored previously. Amazingly, the zero-energy bouquet is characterized by three distinct topological invariants: the first Chern number of a surface enclosing the whole bouquet, the zeroth Chern numbers of the interiors of the two spheres, and the winding number of a loop enclosing the touching point in the plane of symmetry. (ii) We further show that the structured Weyl points can be physically realized in the quasiparticle excitation spectrum

of a 3D spin-orbit coupled (SOC) fermionic cold-atom superfluid with the Fulde-Ferrell (FF) ground state. FF superfluids [30–41] have been studied recently in SOC degenerate Fermi gases subject to Zeeman fields, which yield asymmetries of the Fermi surface and induce the FF Cooper pairing with nonzero total momenta. We obtain a rich phase diagram in the gapless region of 3D FF superfluids, where not only the featureless Weyl points [19–28] but also the structured Weyl points emerge. Note that the featureless Weyl points have been well studied in SOC FF superfluids [24], and here we focus only on the novel structured Weyl points. (iii) We also discuss how the structured Weyl points can be detected in experiments by measuring spectral densities in photoemission spectroscopy that has already been utilized in degenerate Fermi gases [42].

Toy model of structured Weyl point.—Near the Weyl point a Weyl semimetal or superfluid can be described by Weyl Hamiltonian $H_W = \pm \sum_{i=x,y,z} v_i k_i \sigma_i$, where σ_i are Pauli matrices and $\pm$ denote the chirality. Clearly, the two bands disperse linearly and cross only at the Weyl point at the zero energy. Hereafter we will focus on the positive chirality and choose $v_i = 1$ for simplicity. The topological charge of the Weyl point can be characterized by the first Chern number

$$C_2 = \frac{1}{2\pi} \sum_{E_n < 0} \oint_{\mathcal{S}} \Omega_n(\boldsymbol{k}) \cdot d\boldsymbol{S}, \qquad (1)$$

where the surface $\mathcal{S}$ only encloses the considered Weyl point, and $\Omega_n(\boldsymbol{k}) = i\langle \nabla_{\boldsymbol{k}} u_n(\boldsymbol{k})| \times |\nabla_{\boldsymbol{k}} u_n(\boldsymbol{k})\rangle$ is the Berry curvature [43] for the nth band with $|u_n(\boldsymbol{k})\rangle$ being its wave function. For the linearized two-band model, $\Omega_{\mp}(\boldsymbol{k}) = \pm \boldsymbol{k}/2k^3$ and $\mp$ label the eigenvalue of $\sum_i k_i \sigma_i / k$, i.e., the helicity, as depicted in Fig. 1(a). This yields $C_2 = 1$ for Weyl points with positive chirality.

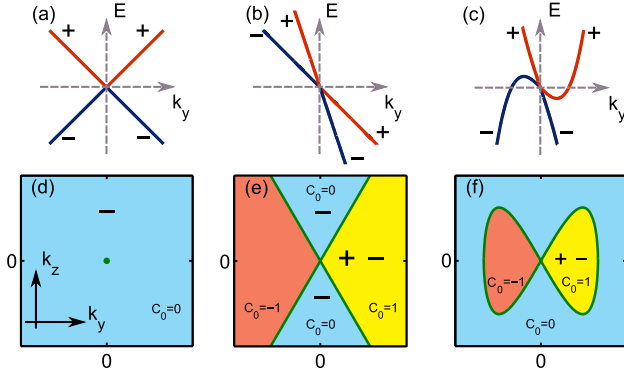To generate a structured Weyl point, we add two new momentum dependent terms in H_W such that

FIG. 1 (color online).   The energy dispersions of H_W along k_y ($k_x = k_z = 0$) for $(\alpha, \gamma) = (0,0)$ in (a), (2,0) in (b), and (2,1) in (c). (d)–(f) plot the distributions of the negative-energy bands in the $k_x = 0$ plane, corresponding to (a)–(c), respectively. The states at the green dots and lines have zero energies. $\pm$ represent the band helicities.

$$H_W = -\alpha k_y \sigma_0 + (k_y + \gamma k_y^3)\sigma_y + k_x \sigma_x + k_z \sigma_z, \quad (2)$$

with α, $\gamma > 0$. The first term that breaks the chiral symmetry along y is $-\alpha k_y \sigma_0$, which does not change the eigenstates and their helicities, leaving the Berry curvatures invariant. However, this term does change the band energies $E_\mp$. With increasing α, the two bands along the k_y axis rotate clockwise. When $\alpha > 1$, the particle and hole portions are inverted for the band with positive velocity, as shown in Fig. 1(b). Since the helicity $+$ and $-$ bands are both occupied at the same momentum and their Berry curvatures are opposite, their contributions to C_2 become vanishing. In Figs. 1(d) and 1(e), we plot the distribution of the occupied-band helicities in the $k_x = 0$ plane. For $\alpha > 1$, both $+$ and $-$ bands are occupied in the yellow region when $k_y > \sqrt{(k_x^2 + k_z^2)/(\alpha^2 - 1)}$, whereas no band is occupied in the mirror reflected red region. This is in sharp contrast to the case for $\alpha < 1$, where only the $-$ band is occupied beyond the Weyl point. Evidently, C_2 is suppressed and not quantized for $\alpha > 1$, which is anomalous.

To restore a quantized C_2, we add the cubic term to regularize H_W. It follows that the band energies become $E_\pm = -\alpha k_y \pm E_0$ with $E_0 = \sqrt{(k_y + \gamma k_y^3)^2 + k_x^2 + k_z^2}$, and that the Berry curvatures read $\Omega_{\mp,x} = \pm k_x(1 + 3\gamma k_y^2)/2E_0^3$, $\Omega_{\mp,y} = \pm k_y(1 + \gamma k_y^2)/2E_0^3$, and $\Omega_{\mp,z} = \pm k_z(1 + 3\gamma k_y^2)/2E_0^3$. At large k_y the cubic term changes faster than the linear terms, resulting in a finite zero-energy surface, as sketched in Figs. 1(c) and 1(f), instead of an infinite cone structure. This suggests that a Weyl point can develop a pair of nondegenerate gapless spheres, i.e., a *bouquet of two spheres*. We further obtain $C_2 = 1$, as long as the surface $\mathcal{S}$ in Eq. (1) encloses the whole bouquet.

Apart from the first Chern number C_2, intriguingly, there exist two additional topological invariants characterizing the whole bouquet. In the $k_y = 0$ plane, there is a chiral symmetry $\sigma_y H_W \sigma_y = -H_W$ and thus in general H_W can be transformed into an off-diagonal block form $\{\{0, h(\mathbf{k})\}, \{h(\mathbf{k})^\dagger, 0\}\}$ with a winding number defined as

$$C_1 = -\frac{1}{2\pi i} \oint_{\mathcal{L}} \mathrm{Tr}[h(\mathbf{k})^{-1}\mathbf{d}h(\mathbf{k})] \in \mathbb{Z}, \quad (3)$$

for a loop $\mathcal{L}$ around the band crossing node [44–46]. Direct calculation yields $C_1 = 1$ in our case, and the corresponding Berry phase is π. Moreover, the whole bouquet divides the momentum space into three regions with full energy gaps. Any point $\mathcal{P}$ in these regions is characterized by its zeroth Chern number [44], which reads

$$C_0 = \frac{1}{2}\left[\sum_{E_n<0}\langle u_n(\mathcal{P})|u_n(\mathcal{P})\rangle - \sum_{E_n>0}\langle u_n(\mathcal{P})|u_n(\mathcal{P})\rangle\right]. \quad (4)$$

C_0 amounts to half of the number difference between the occupied and unoccupied bands since the 0D manifold is featureless in momentum. We find that in the interior $C_0 = 1$ ($C_0 = -1$) for $k_y > 0$ ($k_y < 0$) whereas in the exterior $C_0 = 0$. Therefore, the whole bouquet can be characterized by (C_0, C_1, C_2).

Realization in 3D FF superfluids.—The toy model, Eq. (2), may be applied to describe the band structures of solid-state materials or the quasiparticle spectra in superfluids or superconductors. Here we explore the latter possibility in realizing the structured Weyl points in a 3D SOC degenerate Fermi gas subject to Zeeman fields, where the dominant ground state phase is the FF superfluid [30–34].

We consider a 3D Fermi gas with a Rashba SOC and an attractive s-wave contact interaction. Based on a standard mean-field approximation [33], the thermodynamical potential is $\Omega = |\Delta_0|^2/U + \sum_{\mathbf{k}}(\varepsilon_{\mathbf{k}-\mathbf{Q}/2} - \mu) - \sum_{\mathbf{k},\sigma}(2\beta)^{-1}\ln(1 + e^{-\beta E_{\mathbf{k}\sigma}})$. Here U is the interaction strength [47], $\beta = 1/k_B T$ is the inverse of temperature, $\varepsilon_{\mathbf{k}} = \hbar^2\mathbf{k}^2/2m$ is the kinetic energy, μ is the chemical potential, $\mathbf{Q}$ is the finite momentum of Cooper pairs with an FF order strength Δ_0, and $E_{\mathbf{k}\sigma}$ are the eigenenergies of the Bogoliubov–de Gennes (BdG) Hamiltonian

$$H_{BdG} = [\varepsilon_{\mathbf{k}} - \bar{\mu} + \lambda(\boldsymbol{\sigma} \times \mathbf{k}) \cdot \hat{z}]\tau_z + \Delta_0 \tau_x$$
$$+ \bar{h}_x \sigma_x + h_z \sigma_z + \hbar^2 k_y Q_y/2m, \quad (5)$$

with $\bar{\mu} = \mu - Q_y^2\hbar^2/8m$ and $\bar{h}_x = h_x + \lambda Q_y/2$. In Eq. (5), the Pauli matrices $\boldsymbol{\sigma}$ and $\boldsymbol{\tau}$ act on the spin and the Nambu spaces, h_x and h_z are the in-plane and the out-of-plane Zeeman fields, λ is the SOC strength, and the basis is chosen as $(c_{\mathbf{k}+\mathbf{Q}/2\uparrow}, c_{\mathbf{k}+\mathbf{Q}/2\downarrow}, c_{-\mathbf{k}+\mathbf{Q}/2\downarrow}^\dagger, -c_{-\mathbf{k}+\mathbf{Q}/2\uparrow}^\dagger)^T$ with $\mathbf{Q} = Q_y\hat{y}$ [30,48]. To obtain the self-consistent mean-field solutions of Δ_0, Q_y, and μ, we solve the nonlinear saddle point equations $\partial\Omega/\partial\Delta_0 = 0$ and $\partial\Omega/\partial Q_y = 0$, and the

atom number equation $\partial\Omega/\partial\mu = -n$ with a conserved total atom density n.

To shed light on how the Weyl nodes emerge and evolve in the BdG spectrum, we first analyze the symmetries of the physical system beyond the intrinsic particle-hole symmetry ($\Xi = \sigma_y\tau_y K$ with K the complex conjugation). When $h_{x,z} = 0$, the time-reversal symmetry ($\Theta = \sigma_y K$) is present, and the mirror symmetries ($\mathcal{M}_\nu = -i\sigma_\nu$, $\nu = x, y$) are also unbroken by the SOC or the pairing, i.e., $\mathcal{M}_\nu^{-1} H_{BdG} \mathcal{M}_\nu = H_{BdG}(-k_\nu)$. When the Zeeman fields $h_{x,z}$ are turned on, the time-reversal and the two mirror symmetries are broken explicitly, since there are terms in the second line of Eq. (5) which are odd under their individual operations. Yet, these terms are still even under the product operations of Θ and $\mathcal{M}_y$. Therefore, independent of the presence of Zeeman fields, $\Pi = \Xi\Theta\mathcal{M}_y = i\sigma_y\tau_y$ is an effective symmetry of the system, i.e., $\Pi^{-1}H_{BdG}\Pi = -H_{BdG}(-k_y)$. Similarly, without h_x fields (thus $Q_y = 0$), $\mathcal{M} = \Theta\mathcal{M}_x$ is an extra symmetry, because of $\mathcal{M}^{-1}H_{BdG}\mathcal{M} = H_{BdG}(-k_y, \pm k_z)$ [considering the intrinsic symmetry $H_{BdG} = H_{BdG}(-k_z)$].

The h_x Zeeman field is critical for the presence of structured Weyl points. When $h_x = 0$, the two symmetries, Π and $\mathcal{M}$, dictate that any zero-energy state of a *dispersed* band must have a zero-energy partner state at the same momentum. This indicates that a doubly degenerate Weyl node can exist whereas a nondegenerate state cannot stay at the zero energy. When $h_x \neq 0$, the $\mathcal{M}$ symmetry is broken, and the double degeneracy for gapless states is only dictated in the $k_y = 0$ plane. Indeed, we find that in the phase diagram two or four Weyl nodes can appear in this plane, and each can evolve into a band crossing node with a nondegenerate gapless surface structure developed on each side of the plane. For Eq. (5), a pair of band crossing nodes appears when $h_z^2 > \bar{\mu}^2 + \Delta_0^2 - \bar{h}_x^2$, and two pairs appear when $\Delta_0^2 - \bar{h}_x^2 < h_z^2 < \bar{\mu}^2 + \Delta_0^2 - \bar{h}_x^2$ and $\bar{\mu} > 0$. We map out the zero-temperature phase diagram across the BCS-BEC crossover as a function of h_z in Fig. 2(a) and a function of h_x in Fig. 2(b). The FF superfluids of finite-momentum Cooper pairs are dominant except in a region deep into the BEC side. In sharp contrast to the superfluids without the h_x field where only Weyl points can exist, these superfluids can also possess structured Weyl points, as plotted in Fig. 2(c).

As discussed in the toy model, a structured Weyl node can be characterized by three independent topological invariants (C_0, C_1, C_2). We find that $C_2 = -1$ ($C_2 = 1$) for a closed surface enclosing the whole bouquet at $k_z > 0$ ($k_z < 0$). This reflects that the gapless bouquet originates from a Weyl node. Furthermore, in the $k_y = 0$ plane, there is a chiral symmetry $\Pi^{-1}H_{BdG}\Pi = -H_{BdG}$, and based on Eq. (3) the winding number $C_1 = 1$ and the corresponding Berry phase is π. Intriguingly, for each bouquet, the nondegenerate gapless surface separates the momentum space into three topologically distinct regions with different
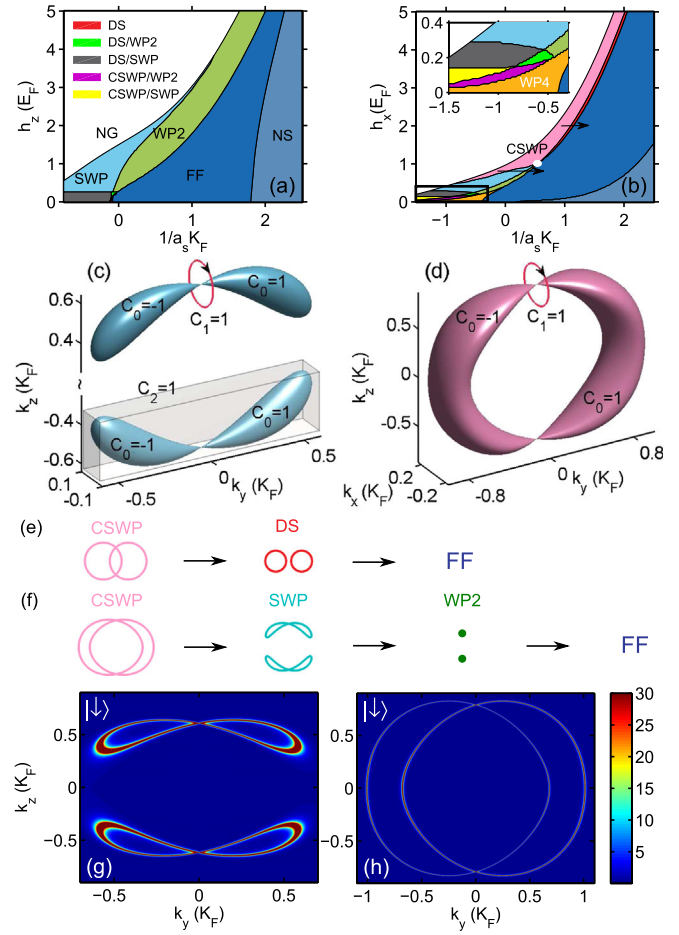

FIG. 2 (color online). Phase diagrams across the BCS-BEC crossover for $h_x = 0.5E_F$ in (a) and for $h_z = 0.4E_F$ in (b). The inset [49] enlarges the black rectangular area. Zero-energy contours for a pair of SWPs in (c) and for a CSWP in (d). (e) and (f) sketch the evolutions of the zero-energy contours in the $k_x = 0$ plane along the arrows above and below the multicritical point (the white point). (g) and (h) show the spin-down quasiparticle spectral densities in the $k_x = 0$ plane for (c) and (d). The Fermi energy E_F is $\hbar^2 K_F^2/2m$ with $K_F = (3\pi^2 n)^{1/3}$. WP2: two Weyl points; WP4: four Weyl points; SWP: structured Weyl point; CSWP: connected structured Weyl points; DS: disconnected spheres; NS: normal superfluids with $Q_y < 10^{-4}K_F$; NG: normal gases. Here $\lambda K_F = E_F$.

C_0 indices. In the exterior $C_0 = 0$ whereas in the interior $C_0 = 1$ ($C_0 = -1$) on the $k_y > 0$ ($k_y < 0$) sides. This result is consistent with the Π symmetry that relates the positive and negative energy bands at opposite k_y. Evidently, a whole bouquet has topological invariants ($\pm 1, \pm 1, \pm 1$). As we have observed, all these unique features of the structured Weyl node have been exhibited in our toy model, Eq. (2).

As the interaction strength or the Zeeman field strength changes, the gapless spheres of different bouquets can even connect and merge together as long as their C_0 indices are the same. An example of such a connected bouquet (i.e., CSWP phase) is shown in Fig. 2(d). The two bouquets have opposite C_2 indices before their merging, and hence any
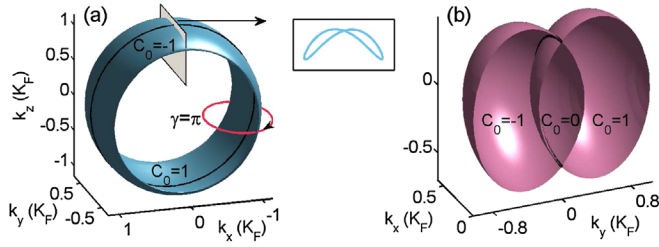
FIG. 3 (color online).   (a) Zero-energy contours of a structured Weyl ring (SWR). The inset shows the cross section of a SWR. (b) A closed SWR (CSWR). Only $k_x > 0$ part is plotted; the $k_x < 0$ part is symmetric to the $k_x > 0$ part with respect to the $k_x = 0$ plane. Here $\lambda K_F = E_F$.

surface enclosing the whole connected bouquet has $C_2 = 0$ after merging. Yet, the winding number C_1 of any loop enclosing either band crossing node in the $k_y = 0$ plane as well as the zeroth Chern number C_0 are still intact. Thus, a connected bouquet has topological invariants $(\pm 1, \pm 1, 0)$.

There exists a multicritical point (the white point) in Fig. 2(b) where five distinct phases intersect and the gap closes at $\mathbf{k} = 0$. Increasing $1/a_s K_F$ for a fixed h_z above and below the multicritical point represents two different processes of destroying the phase with a connected bouquet. For the larger h_x, as the interaction increases, the two band crossing nodes of the connected bouquet move toward each other along $\hat{k}_z$ and then pair-annihilate, leading to a gapless FF phase with two disconnected spheres (i.e., DS phase in Fig. 2) located at two sides of the $k_y = 0$ plane. As the interaction further increases, the spheres shrink and eventually disappear, yielding a gapped FF superfluid. This process is sketched in Fig. 2(e). The other process for the smaller h_x is sketched in Fig. 2(f). As the interaction increases, the connected bouquet is first broken down into a pair of disconnected bouquets, then each shrinks into a Weyl node, and eventually the two Weyl nodes pari-annihilate at $\mathbf{k} = 0$ producing a gapped FF superfluid. Intriguingly, each gapless phase has at least one topological invariant.

Structured Weyl ring.—Given the existence of structured Weyl points, one may wonder whether there exist structured Weyl rings in 3D. We can construct a simple model to describe such a ring: $H_{\text{WR}} = -\alpha k_y \sigma_0 + (k_y + \gamma k_y^3)\sigma_y + (\mathbf{k}^2 - m^2)\sigma_z$ with nonzero m. Analogous to structured Weyl points, when $\alpha > 1$ and $\gamma > 0$, the zero-energy contour is a structured Weyl ring; i.e., a bouquet of two circles travels along a loop as shown in Fig. 3(a). Although the first Chern number C_2 for a surface enclosing the whole ring is zero, the Berry phase along the loop trajectory enclosing the ring is $\gamma = \pi$ [50] and the zeroth Chern numbers C_0 of the gapped interiors are quantized to ± 1. Such a structured Weyl ring can indeed be realized in the quasiparticle spectrum of SOC FF superfluids, with equal Rashba and Dresselhaus SOC, i.e., the model, Eq. (5), with the Rashba SOC replaced by $H_{\text{SOC}}(\hat{\mathbf{p}}) = \lambda \hat{p}_y \sigma_x$ [51].

Here Π symmetry and rotational symmetry with respect to k_y $[H_{\text{BdG}} = H_{\text{BdG}}(k_x^2 + k_z^2, k_y)]$ dictate that crossing rings can exist in the $k_y = 0$ plane. Indeed, in this plane for FF superfluids with a h_x field, a ring appears when $h_z^2 > \bar{\mu}^2 + \Delta_0^2 - \bar{h}_x^2$, and two rings appear when $\Delta_0^2 - \bar{h}_x^2 < h_z^2 < \bar{\mu}^2 + \Delta_0^2 - \bar{h}_x^2$ and $\bar{\mu} > 0$. Similar to the case for structured Weyl points, $\mathcal{M}$ symmetry is broken by h_x fields so that the Weyl ring can develop structures on both sides of the $k_y = 0$ plane, as shown in Fig. 3(a). The developed gapless contours can further bend toward $k_x = k_z = 0$ and become closed, as shown in Fig. 3(b). It follows that then only C_0 is responsible for the protection of the zero-energy structures.

Experimental observation.—To observe the structured Weyl nodes or rings, we consider the quasiparticle spectral density $A_\sigma(\omega, \mathbf{k}) = -\text{Im}G_{\sigma\sigma}(i\omega = \omega + i\delta, \mathbf{k})/\pi$, where $G = (i\omega - H_{\text{BdG}})^{-1}$ is the Green function. $A_\sigma(\omega, \mathbf{k})$ can be experimentally measured using the spin and momentum resolved photoemission spectroscopy [42]. To evaluate the zero-energy spectral density, we compute $A_\downarrow(\omega = 0, \mathbf{k})$ in the $k_x = 0$ plane, which is illustrated in Figs. 2(g) and 2(h) for a pair of structured Weyl nodes. The signal of $A_\uparrow(\omega = 0, \mathbf{k})$ is similar, though it has a weaker amplitude due to the smaller particle density. For a structured Weyl ring, the signal of A_σ in the $k_x = 0$ plane is similar to that of the structured Weyl node, but exhibits a ring structure in the $k_y = 0$ plane instead of two points for a pair of structured Weyl nodes. We note that a structured Weyl node or ring also has an interesting surface spectral density [25]. In experiments, SOC and Zeeman fields have been recently realized [52–60] in ^{40}K and ^{6}Li fermionic atoms by coupling two hyperfine states via counterpropagating Raman laser beams. The SOC strength is determined by the wavelength l_r of the Raman beams and their relative angle θ by $\lambda K_F = 2(k_r \sin(\theta/2)/K_F)E_F$ with $k_r = 2\pi/l_r$. This strength can be as large as $\lambda K_F = 2E_F$ when we consider a typical set of parameters: $l_r = 773$ nm and $n = 1.8 \times 10^{13}$ cm^{-3} [53]. The Zeeman fields, depending on the laser beam strength or the detuning, can also be readily tuned to E_F. These parameters are large enough to observe the exotic Weyl phases discovered here. We note that in a harmonic trap, the quasiparticle spectrum around the center of the trap can be measured using spatially resolved photoemission spectroscopy assisted by hollow light technology [61].

In summary, we demonstrate that a Weyl point in semimetals or nodal superfluids can deform into a bouquet of two spheres. We show that such a structured Weyl point is characterized by three distinct topological invariants and can be realized in SOC Fermi gases subject to Zeeman fields. Such nontrivial structured Weyl points have not been discussed previously in ^{3}He or other topological superconductors or superfluids. Our discovery introduces a new class of topological quantum matter and may have great impact in both cold-atom and solid-state communities.

Note added.—Recently, we noticed two newly posted preprints [62,63] on a new type of Weyl point and its realization in the single particle band dispersion of certain solid materials (e.g., WTe$_2$ and MoTe$_2$), where the Weyl Hamiltonian around the Weyl point is similar to our toy Hamiltonian Eq. (2) with only linear terms considered.

---

*chuanwei.zhang@utdallas.edu

[1] H. Weyl, Zeitschrift für Physik **56**, 330 (1929).
[2] G. E. Volovik, *The Universe in a Helium Droplet* (Clarendon Press, Oxford, 2003).
[3] S. Murakami, New J. Phys. **9**, 356 (2007).
[4] X. Wan, A. M. Turner, A. Vishwanath, and S. Y. Savrasov, Phys. Rev. B **83**, 205101 (2011).
[5] K.-Y. Yang, Y.-M. Lu, and Y. Ran, Phys. Rev. B **84**, 075129 (2011).
[6] A. A. Burkov and L. Balents, Phys. Rev. Lett. **107**, 127205 (2011).
[7] G. Xu, H. Weng, Z. Wang, X. Dai, and Z. Fang, Phys. Rev. Lett. **107**, 186806 (2011).
[8] V. Aji, Phys. Rev. B **85**, 241101(R) (2012).
[9] A. A. Zyuzin, S. Wu, and A. A. Burkov, Phys. Rev. B **85**, 165110 (2012).
[10] C. Fang, M. J. Gilbert, X. Dai, and B. A. Bernevig, Phys. Rev. Lett. **108**, 266802 (2012).
[11] L. Lu, L. Fu, J. D. Joannopoulos, and M. Soljačić, Nat. Photonics **7**, 294 (2013).
[12] P. Hosur and X. Qi, C.R. Phys. **14**, 857 (2013).
[13] O. Vafek and A. Vishwanath, Annu. Rev. Condens. Matter Phys. **5**, 83 (2014).
[14] H. Weng, C. Fang, Z. Fang, B. A. Bernevig, and X. Dai, Phys. Rev. X **5**, 011029 (2015).
[15] S.-M. Huang, S.-Y. Xu, I. Belopolski, C.-C. Lee, G. Chang, B. Wang, N. Alidoust, G. Bian, M. Neupane, A. Bansil, H. Lin, and M. Z. Hasan, Nat. Commun. **6**, 7373 (2015).
[16] L. Lu, Z. Wang, D. Ye, L. Ran, L. Fu, J. D. Joannopoulos, and M. Soljačić, Science **349**, 622 (2015).
[17] X.-Y. Xu, I. Belopolski, N. Alidoust, M. Neupane, C. Zhang, R. Sankar, S.-M. Huang, C.-C. Lee, G. Chang, B. Wang, G. Bian, H. Zheng, D. S. Sanchez, F. Chou, H. Lin, S. Jia, and M. Z. Hasan, Science **349**, 613 (2015).
[18] B. Q. Lv, H. M. Weng, B. B. Fu, X. P. Wang, H. Miao, J. Ma, P. Richard, X. C. Huang, L. X. Zhao, G. F. Chen, Z. Fang, X. Dai, T. Qian, and H. Ding, Phys. Rev. X **5**, 031013 (2015).
[19] M. Gong, S. Tewari, and C. Zhang, Phys. Rev. Lett. **107**, 195303 (2011).
[20] T. Meng and L. Balents, Phys. Rev. B **86**, 054504 (2012).
[21] J. D. Sau and S. Tewari, Phys. Rev. B **86**, 104509 (2012).
[22] T. Das, Phys. Rev. B **88**, 035444 (2013).

[23] K. Seo, C. Zhang, and S. Tewari, Phys. Rev. A **87**, 063618 (2013).
[24] Y. Xu, R.-L. Chu, and C. Zhang, Phys. Rev. Lett. **112**, 136402 (2014).
[25] S. A. Yang, H. Pan, and F. Zhang, Phys. Rev. Lett. **113**, 046401 (2014).
[26] P. Goswami and L. Balicas, arXiv:1312.3632.
[27] H. Hu, L. Dong, Y. Cao, H. Pu, and X.-J. Liu, Phys. Rev. A **90**, 033624 (2014).
[28] B. Liu, X. Li, L. Yin, and W. V. Liu, Phys. Rev. Lett. **114**, 045302 (2015).
[29] A. Hatcher, *Algebraic Topology* (Cambridge University Press, Cambridge, England, 2002).
[30] Z. Zheng, M. Gong, X. Zou, C. Zhang, and G. Guo, Phys. Rev. A **87**, 031602(R) (2013).
[31] F. Wu, G. C. Guo, W. Zhang, and W. Yi, Phys. Rev. Lett. **110**, 110401 (2013).
[32] X.-J. Liu and H. Hu, Phys. Rev. A **87**, 051608(R) (2013).
[33] L. Dong, L. Jiang, and H. Pu, New J. Phys. **15**, 075014 (2013).
[34] Y. Xu and C. Zhang, Int. J. Mod. Phys. B **29**, 1530001 (2015).
[35] C. Qu, Z. Zheng, M. Gong, Y. Xu, L. Mao, X. Zou, G. Guo, and C. Zhang, Nat. Commun. **4**, 2710 (2013).
[36] W. Zhang and W. Yi, Nat. Commun. **4**, 2711 (2013).
[37] X.-J. Liu and H. Hu, Phys. Rev. A **88**, 023622 (2013).
[38] C. Chen, Phys. Rev. Lett. **111**, 235302 (2013).
[39] C. F. Chan and M. Gong, Phys. Rev. B **89**, 174501 (2014).
[40] Y. Cao, S.-H. Zou, X.-J. Liu, S. Yi, G.-L. Long, and H. Hu, Phys. Rev. Lett. **113**, 115302 (2014).
[41] Y. Xu and C. Zhang, Phys. Rev. Lett. **114**, 110401 (2015).
[42] J. T. Stewart, J. P. Gaebler, and D. S. Jin, Nature (London) **454**, 744 (2008).
[43] D. Xiao, M.-C. Chang, and Q. Niu, Rev. Mod. Phys. **82**, 1959 (2010).
[44] J. C. Y. Teo and C. L. Kane, Phys. Rev. B **82**, 115120 (2010).
[45] F. Zhang and C. L. Kane, Phys. Rev. B **90**, 020501(R) (2014).
[46] J. Song and E. Prodan, Phys. Rev. B **89**, 224203 (2014).
[47] The interaction strength U can be obtained via a standard renormalization procedure, i.e., $U^{-1} = m/(4\pi\hbar^2 a_s) - \int m/(\hbar^2 k^2)d^3\mathbf{k}/(2\pi)^3$, where the s-wave scattering length a_s regularizes the ultraviolet divergence. See S. Giorgini, L. P. Pitaevskii, and S. Stringari, Rev. Mod. Phys. **80**, 1215 (2008).
[48] Y. Xu, C. Qu, M. Gong, and C. Zhang, Phys. Rev. A **89**, 013607 (2014).
[49] For the superfluids with four crossing points, there are five phases in the phase diagram: WP4, CSWP/WP2, CSWP/SWP, DS/WP2, and DS/SWP. The phase name consists of two parts: the former containing the inner crossing points while the latter the outer ones.
[50] X.-L. Qi, T. L. Hughes, and S.-C. Zhang, Phys. Rev. B **78**, 195424 (2008).
[51] K. Seo, L. Han, and C. A. R. Sá de Melo, Phys. Rev. Lett. **109**, 105303 (2012).
[52] Y.-J. Lin, K. Jiménez-García, and I. B. Spielman, Nature (London) **471**, 83 (2011).

[53] P. Wang, Z.-Q. Yu, Z. Fu, J. Miao, L. Huang, S. Chai, H. Zhai, and J. Zhang, Phys. Rev. Lett. **109**, 095301 (2012).

[54] L. W. Cheuk, A. T. Sommer, Z. Hadzibabic, T. Yefsah, W. S. Bakr, and M. W. Zwierlein, Phys. Rev. Lett. **109**, 095302 (2012).

[55] J.-Y. Zhang, S.-C. Ji, Z. Chen, L. Zhang, Z.-D. Du, B. Yan, G.-S. Pan, B. Zhao, Y.-J. Deng, H. Zhai, S. Chen, and J.-W. Pan, Phys. Rev. Lett. **109**, 115301 (2012).

[56] C. Qu, C. Hamner, M. Gong, C. Zhang, and P. Engels, Phys. Rev. A **88**, 021604(R) (2013).

[57] R. A. Williams, M. C. Beeler, L. J. LeBlanc, K. Jiménez-García, and I. B. Spielman, Phys. Rev. Lett. **111**, 095301 (2013).

[58] V. Galitski and I. B. Spielman, Nature (London) **494**, 49 (2013).

[59] J. Zhang, H. Hu, X.-J. Liu, and H. Pu, Ann. Rev. Cold Atoms and Molecules **2**, 81 (2014).

[60] L. Huang, Z. Meng, P. Wang, P. Peng, S.-L. Zhang, L. Chen, D. Li, Q. Zhou, and J. Zhang, arXiv:1506.02861.

[61] J. P. Gaebler, PhD thesis, University of Colorado, 2010.

[62] A. A. Soluyanov, D. Gresch, Z. Wang, Q. Wu, M. Troyer, X. Dai, and B. A. Bernevig, Nature (London) **527**, 495 (2015).

[63] Y. Sun, S.-C. Wu, M. N. Ali, C. Felser, and B. Yan, Phys. Rev. B **92**, 161107 (2015).